IEEE Photonics Journal
An IEEE Photonics Society Publication

Open Access

Realization of Multitone Continuous Wave Lidar

Volume 11, Number 4, August 2019

Rasul Torun
Mustafa M. Bayer
Imam U. Zaman
Jose E. Velazco
Ozdal Boyraz

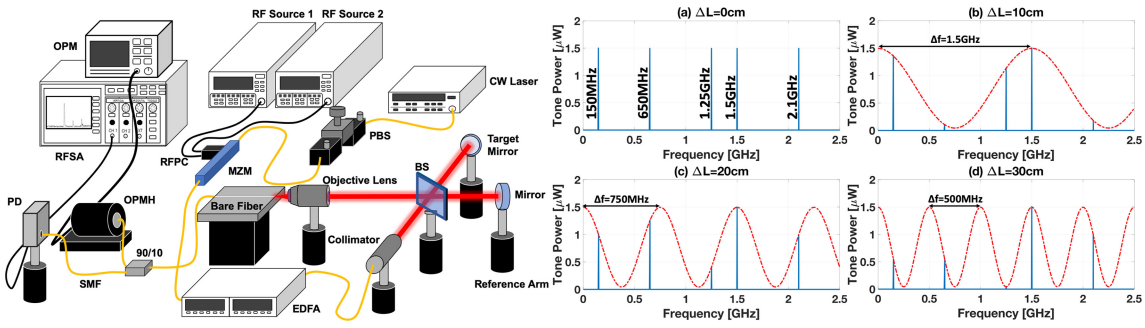

DOI: 10.1109/JPHOT.2019.2922690
1943-0655 © 2019 IEEE

Realization of Multitone Continuous Wave Lidar

Rasul Torun,[1] **Mustafa M. Bayer**,[1] **Imam U. Zaman**,[1] **Jose E. Velazco**,[2] **and Ozdal Boyraz** [1]

[1]Electrical Engineering and Computer Science Department, University of California, Irvine, CA 92697 USA
[2]Jet Propulsion Laboratory, Pasadena, CA 91109 USA

DOI:10.1109/JPHOT.2019.2922690

Manuscript received April 17, 2019; revised May 22, 2019; accepted June 7, 2019. Date of publication June 13, 2019; date of current version July 19, 2019. This work was supported in part by the National Aeronautics and Space Administration (NNX16AT64A) and in part by Office of Naval Research (ONR) (N00014-18-1-2845). Corresponding author: Ozdal Boyraz (e-mail: oboyraz@uci.edu).

Abstract: We have developed a multitone modulated continuous wave (MTCW) Lidar system made of a CW laser with multiple fixed RF tones for a high precision range finding and velocimetry. In this paper, the MTCW Lidar system has been studied analytically and numerically. A proof-of-concept experiment by employing 1550-nm light source and multiple radio-frequency (RF) tone modulations ranging from 50 MHz to 6 GHz has been performed to demonstrate proof of principle for range finding with $<$1-cm range resolution. We also provide sine fitting algorithms on the measured RF tones to extract the range information in a single shot RF measurement and demonstrate the ways to improve the resolution beyond the actual RF bandwidth.

Index Terms: Lidar, range finding, velocimetry, RF modulation, multi-tone modulation, heterodyne detection, interference.

1. Introduction

Light detection and ranging (Lidar) has been used in various ways such as military applications [1] and atmospheric sciences [2] to detect remote objects, measure distances [3], create topographical images [4], detect aerosol particles [5], [6], and measure ozone layers [7], [8]. In recent years, with the advent of self-driving cars and unmanned aerial vehicles (UAV), Lidar became a topic of interest once again for proximity sensing and collision prevention [9]–[14]. However, most of these recent research activities focus on the receiver architectures [15], and signal processing techniques [16], [17] to achieve more robust, accurate and sensitive measurements in longer ranges. Optical backbone mostly relies on Lidar technologies based on pulsed time of flight (PToF) measurements, which transmits laser impulses and collects the scattered light from a target. The measured time delay between transmission and the reception reveals the range information by using simple calculations. To achieve accurate timing, PToF Lidars require short pulse generation and high temporal resolution, which creates the necessity of fast electronics. Therefore, several consecutive measurements are performed in combination with Monte Carlo methods to minimize the error in timing. Additionally, the precision of this approach degrades with distance, also it lacks the ability to detect velocity and direction of moving targets simultaneously [18].

Recently, new Lidar technologies employing continuous wave (CW) lasers emerged as in amplitude modulated continuous wave (AMCW), and frequency modulated continuous wave (FMCW) Lidars [19]–[21]. The AMCW Lidars modulate the intensity of the light while keeping the frequency constant. Depending on the desired measurement precision, AMCW technique requires high-speed radio-frequency (RF) electronics to modulate the light intensity. On the receiver side, this requirement can be mitigated via demodulation or superheterodyne receivers that can convert the high-frequency tones into base-band signals. The range information is either obtained by convolving the local oscillator with the time-delayed return signal as in phase shift Lidars, or electronic heterodyne detection to generate a beat note proportional to the target distance as in linearly chirped Lidars [18], [19]. Previously, $<$5 mm precision was reported for distances $<$12 m by employing AMCW Lidars and precision improvement techniques such as multiple signal classification and harmonic distortion cancellation [22]–[24].

Moreover, the FMCW Lidars are based on frequency sweeping of the light sources such as tunable lasers or frequency modulated CW lasers with a chirped RF signal. The backscattered signal is detected via optical heterodyning that employs a slow square-law detector, therefore the generated beating frequency can be recorded by slower electronics [18]. Since the same target is measured with several frequencies, the results are more robust and accurate [19]. Also, they have the potential of detecting the speed and direction of the target simultaneously [25], [26]. The FMCW Lidar systems can achieve sub-mm resolutions for shorter ranges ($<$10 m), while utilizing wide-band frequency tuning via swept sources [27]–[29]. The resolution degrades to $\sim$5 cm at medium ranges ($\sim$100 m), with a bandwidth that is limited to 5 GHz [30]. However, in the practical domain, frequency stability of the laser source and technical challenges limit the sweeping frequency range up to a few GHz, therefore the range resolution is limited to cm level, which mitigates the reliability of frequency chirped Lidars [31], [32]. Very recently, frequency combs are utilized to achieve $>$THz bandwidth with μm resolutions in shorter ranges, as well [33]. On the other hand, some frequency domain Lidars previously employed the multiple-wavelength techniques such as continuous time-of-flight measurements [34], multi-wavelength super-heterodyning [35], [36] and multi-frequency demodulation via CMOS photonic mixer devices [37], which were used for short-range and high precision imaging and ranging. However, it is important to note that these efforts are mainly targeted for short-range measurements in applications such as Microsoft Kinect.

In addition to AMCW and FMCW, phase-based ranging is also a remarkable technique for absolute metrology systems [38]. However, implementation of such a system is troublesome due to the requirement of multiple detectors or detector arrays, as well as heterodyne detection of two arms with different frequencies. Also, the detection in such applications requires either phase detectors or elaborates phase extraction techniques during post-processing. Lack of direct velocity measurement is another drawback of such techniques. Therefore, a less burdensome system is necessary with high-resolution capability for longer ranges that can also provide the velocity information simultaneously.

Here, we present a multi-tone modulated continuous wave (MTCW) Lidar technology that can provide high precision range and velocity information of static and moving targets. In the proposed approach, CW lasers are simultaneously modulated with a few carefully selected RF tones. At the receiver, the interference of the scattered light with the reference is detected by a photodiode. Since, the acquired light travels to the target and back to the beam splitter, the interference signal carries the range and velocity information of the target at the amplitude and phase of the detected RF tones. We utilize the relative amplitude variations in RF tones to extract the range and velocity information. In this manuscript, the proposed MTCW Lidar system is investigated theoretically and verified with numerical simulations. Also, a proof of principle experiment has been performed for ranging of a static target. We show the short distance range measurements with $<$1 cm accuracy by using 2.5 GHz and 6 GHz RF tones. The accuracy can be further improved by increasing the tone frequencies, data extrapolation, and signal processing algorithms. Recent progress in the development of highly coherent narrow linewidth lasers allows practical devices that can operate

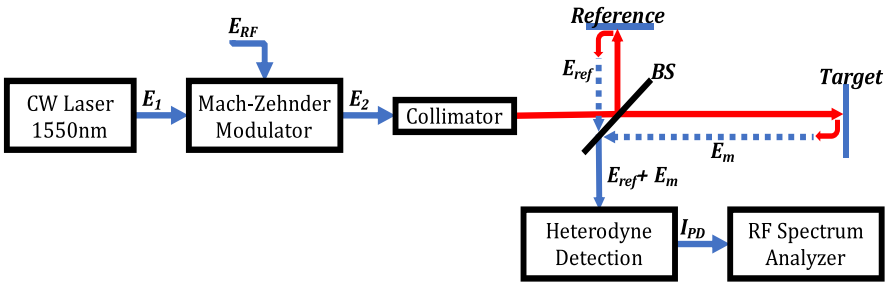

Fig. 1. Schematic of the proposed multi-tone continuous wave Lidar system.

over kilometers of distances. As a result, the proposed method can be suitable for aerial or satellite-based remote sensing applications with cm accuracy.

2. Principle and Numerical Results

Figure 1 illustrates the schematic of the MTCW Lidar system. The system is driven by a CW laser source that is amplitude modulated by a Lithium Niobate ($LiNbO_3$) modulator to create well separated optical tones. The signal is then split into two as the reference and the measurement arms. The measurement signal is incident on the target after collimation and beam expansion. The reflected beam is then collected back at the same transmit aperture or a separate collection aperture. After collecting the reflected signal, it is collimated back and sent to an interferometer that enables the superposition of the transmit signal and the reference signal on a detector. The photodetector is used to detect the interference and create RF tones required for range finding and velocimetry. In particular, we are interested in the relative amplitude variations of modulation tones to extract the range information. Due to the difference in the phase accumulation at different optical tones at a given target distance, we will have nonuniform amplitudes across the RF frequencies. By carefully evaluating the strength of the tone powers, we can estimate the path length covered by the optical beam from the source, to the target and back to the detector. In this study, we have developed an algorithm that recognizes the amplitude nonuniformity across the harmonic frequencies and precisely detect the range information from these amplitude variations. If there is a moving target, it is also possible to detect the Doppler shift to identify the velocity and direction with the same configuration. The number of RF tones and their frequencies are selected carefully for the desired range and precision. Consequently, the proposed method is employing multi-tone RF modulation, optical heterodyning and sine fitting algorithms that enable acquisition of range and possible velocity information in a single shot measurement by eliminating the need of frequency, amplitude or phase sweeping.

2.1 Analytical Modeling

The unmodulated complex optical field at the output of the CW laser can be modeled as $E_1 = A_0 \exp(j\omega_0 t + j\phi_0)\exp(-jk_0 z)$ where A_0 is the amplitude of the light's electric field, ω_0 is the angular frequency of the optical carrier, ϕ_0 is the phase of the initial light beam, k_0 is the angular wave number, and z is the propagation distance [39]. Later, this optical carrier is intensity modulated by a waveform that is the sum of sinusoidal signals, $E_{RF} = \sum_{i=1}^{N} A_i \cos(2\pi f_i t + \phi_i) = \sum_{i=1}^{N} 0.5\, A_i[\exp(j2\pi f_i t + j\phi_i) + \exp(-j2\pi f_i t - j\phi_i)]$ where A_i, f_i, and ϕ_i are the amplitude, frequency, and phase of ith RF tone, respectively. The field transfer function of the balanced driven Mach Zehnder modulator (MZM) under push-pull configuration is $\cos(0.5\pi v_m/V_\pi)$ where $v_m = V_\pi/2 + E_{RF}$ at quadrature bias. Therefore, after trigonometric conversions, the transfer function of MZM can be rewritten as $\cos(\frac{\pi}{4} + \frac{\pi}{2V_\pi}E_{RF}) = \frac{1}{\sqrt{2}}\{\cos(\frac{\pi}{2V_\pi}E_{RF}) - \sin(\frac{\pi}{2V_\pi}E_{RF})\}$. To achieve linear modulation, we used low modulation depth ($m = \pi A_i/V_\pi \ll 1$), therefore modulated electric field can be expressed

by $E_2 = \frac{E_1}{\sqrt{2}} - \frac{E_1}{\sqrt{2}} \frac{\pi}{2V_\pi} E_{RF}$ by using small angle approximations. After inserting E_1 and E_{RF},

$$E_2 = \frac{A_0}{\sqrt{2}} \exp\left(j\omega_0 t + j\phi_0 - jk_0 z\right) - \frac{mA_0}{4\sqrt{2}} \left\{ \sum_{i=1}^{N} \exp\left[j\left(\omega_0 + 2\pi f_i\right) t + j\left(\phi_0 + \phi_i\right) - jk_0 z\right] + \exp\left[j\left(\omega_0 - 2\pi f_i\right) t + j\left(\phi_0 - \phi_i\right) - jk_0 z\right] \right\}$$

where all the RF tone amplitudes are selected equal, therefore the modulation depth, m, is the same for all RF tones. Later, modulated light is transferred to the free space through a collimator and split into two via a beam splitter. While one signal is traveling to the target (measurement signal), the other is kept inside the system to be used as a local oscillator (reference signal) in coherent detection. Both signals accumulate phase during propagation, and the returned signals at the detector can be represented as

$$E_{ref,m} = \frac{A_0}{2\sqrt{2}} \alpha_{ref,m} \exp\left(j\omega_0 t + j\phi_0 + j\omega_0 \frac{2L_{ref,m}}{c}\right) - m\frac{A_0}{4\sqrt{2}} \alpha_{ref,m} \left\{ \sum_{i=1}^{N} \exp\left[j\left(\omega_0 + 2\pi f_i\right) t + j\left(\phi_0 + \phi_i\right) + j\left(\omega_0 + 2\pi f_i\right) \frac{2L_{ref,m}}{c}\right] + \exp\left[j\left(\omega_0 - 2\pi f_i\right) t + j\left(\phi_0 - \phi_i\right) + j\left(\omega_0 - 2\pi f_i\right) \frac{2L_{ref,m}}{c}\right] \right\}$$

where L_{ref} and L_m are the distances between the beam splitter – reference mirror and beam splitter – target, respectively. Also, α_{ref} and α_m are the linear loss coefficients of free-space propagation. On the detector, the reference and measurement signals will be mixed, and the current output of the PIN photodiode will be $I_{PD} = RP_{in} = R(E_{ref} + E_m)(E_{ref} + E_m)^*$ where R is the responsivity of the detector and P_{in} is input optical power on the detector. The phase shift of each tone will convert into amplitude variations at different RF tones as:

$$I_{PD} = I_{PD,ave} - \frac{1}{4} RmA_0^2 \sum_{i=1}^{N} \left(\alpha_{ref}^2 + \alpha_{ref}\alpha_m\right) \cos\left(2\pi f_i t + \frac{4\pi}{c} L_{ref} f_i\right) + \left(\alpha_{ref}\alpha_m + \alpha_m^2\right) \cos\left(2\pi f_i t + \frac{4\pi}{c} L_m f_i\right)$$

where $I_{PD,ave}$ is the average photodiode current which is the sum of all self-beating components.

This result assumes that we can ignore higher order distortion tones (HD2, IMD3, etc.) and phase mismatch is generated by only the optical path difference between the reference arm and the measurement arm. We can drive the modulator in the linear regime by keeping modulation depth low. Then, the higher order distortion terms will be suppressed at a much faster rate than the fundamental tones, hence the spur free dynamic range (SFDR) of the system will be improved [40]. Even though it is not straight forward, it may be wiser to optimize modulation depth to utilize distortion tones as extra measurement tools after isolating the intensity variations due to the mixing of tones. If one can overcome the computation complexity, this will improve the tone powers and system accuracy.

As is clear in the I_{PD} equation, each RF frequency tone, f_i, accumulates different phase while the light is traveling towards the target. Therefore, interference of the backscattered light with the reference will produce a difference in amplitudes for different tones. After recording the power of each tone, the data points are fit into a sinusoidal signal to extract the frequencies, where the reference and measurement signals interfere constructively or destructively. The frequency difference between two consecutive peaks, $\Delta f = |f_{p2} - f_{p1}|$, will determine the range information such as $\frac{4\pi}{c}\Delta L\left(f_{p2} - f_{p1}\right) = 2\pi \Rightarrow \Delta L = \frac{c}{2\Delta f}$ where ΔL is the absolute range difference, $\Delta L = |L_m - L_{ref}|$.

In MTCW Lidar, we are specifically interested in the sinusoidal fit over the measured tone powers as shown in Fig. 2. The amplitude of such fitting depends on the experienced loss in the reference and measurement arms. Peak amplitude is achieved when two cosines are in phase and the minimum amplitude is achieved when two cosines are entirely out of phase.

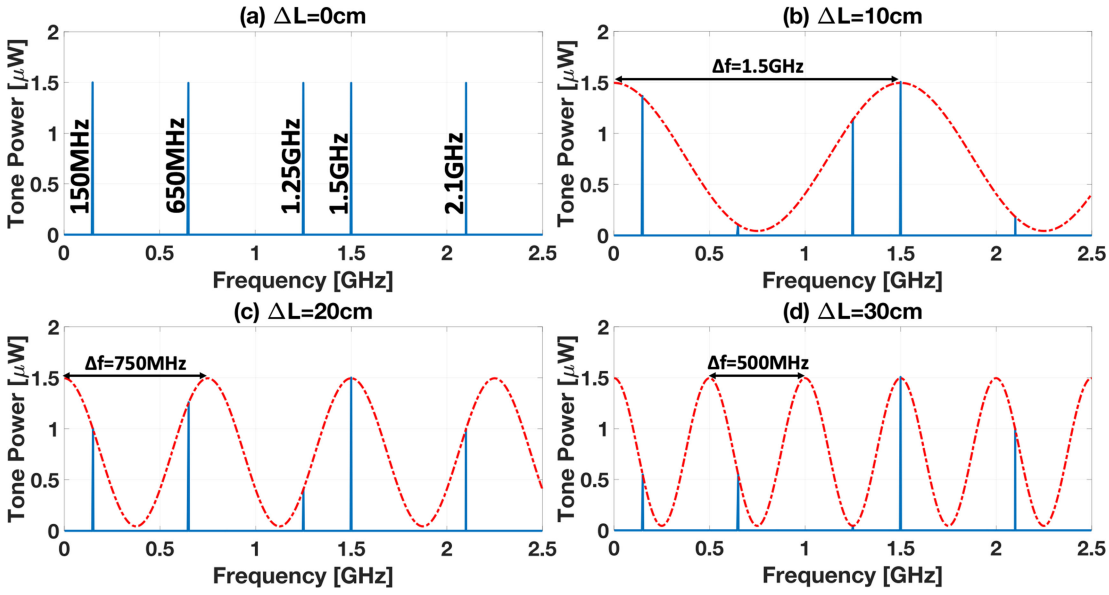

Fig. 2. RF tone power variation for various target distances and corresponding frequencies.

Therefore, the amplitude of modulation is $A_{fit} = 0.25RmA_0^2\alpha_m(\alpha_{ref} + \alpha_m)$, the extinction ratio is $ER = (\alpha_{ref} + \alpha_m)/|\alpha_{ref} - \alpha_m| \overset{if\ \alpha_m \ll \alpha_{ref}}{\rightarrow} 1$ and modulation depth of the oscillation is $m_{osc} = \alpha_m/\alpha_{ref}$. Since the backscattered power from the target is so low, the reference arm should be attenuated to preserve the extinction ratio and modulation depth of the oscillation. However, RF heterodyne detection can be pursued in the electrical domain to further enhance the signal-to-noise ratio (SNR) of the detection system.

2.2 Numerical Verification

We modeled the full system of the proposed MTCW Lidar in the computer environment that includes the modulator and detector nonlinearities, laser and detector noises, and losses in the measurement arm to verify the experimental results. In Fig. 2, the evolution of the tone powers is demonstrated while the range of the target is moved up to 30 cm from its initial position. The modulation depth is set to 10% and losses are neglected ($\alpha_{ref} = \alpha_m = 1$). To eliminate overlapping of actual tones with higher order distortions such as harmonic distortions ($2f, 3f, \ldots$) and intermodulation distortion ($2f_2 \pm f_1, 2f_1 \pm f_2, \ldots$), we selected RF tones as 150 MHz, 650 MHz, 1.25 GHz, 1.5 GHz and 2.1 GHz with the same amplitude as shown in Fig. 2(a). When the target is 10 cm away, the light propagates a total distance of 20 cm back and forth from the target by creating peaks at every 1.5 GHz. While the 1.5 GHz tone has the same amplitude as before, 650 MHz is degraded the most due to the proximity to the valley point at 750 MHz that experience the complete destructive interference at the detector as seen in Fig. 2(b). When the target distance is doubled and tripled as in Fig. 2(c) and Fig. 2(d), respectively, the period of the sinusoidal fit decreases accordingly. Therefore, to achieve high resolutions, larger bandwidth is required. For example, by facilitating 50 GHz RF bandwidth, the system can achieve $<$1 mm resolution. Such higher resolutions can also be achieved by extrapolating the data of the lower frequency tones and signal processing without going to X-band modulation.

When the target range increases, the consecutive peaks of the sinusoidal fit get closer to each other due to inverse proportionality of range and frequency as in $\Delta L = 0.5c/\Delta f$. However, the same modulation pattern repeats itself according to the period of the greatest common divisor (GCD) of all RF tones. For the given tones GCD is 50 MHz, therefore the same modulation pattern is repeating itself in every 3 meters. This MTCW system is designed for the fine range measurements at the

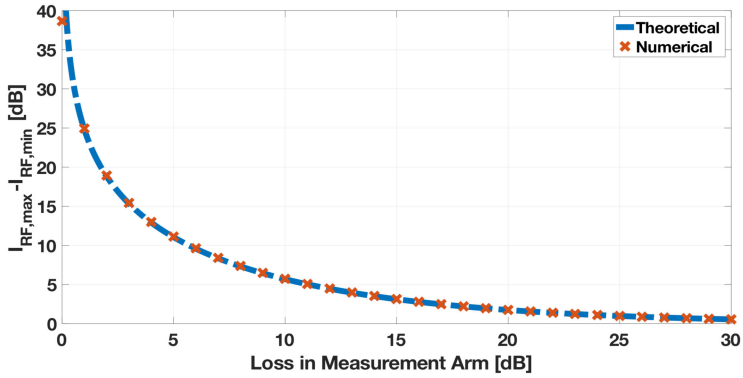

Fig. 3. The effect of measurement arm loss on the modulation depth of sinusoidal fit when there is no loss in the reference arm.

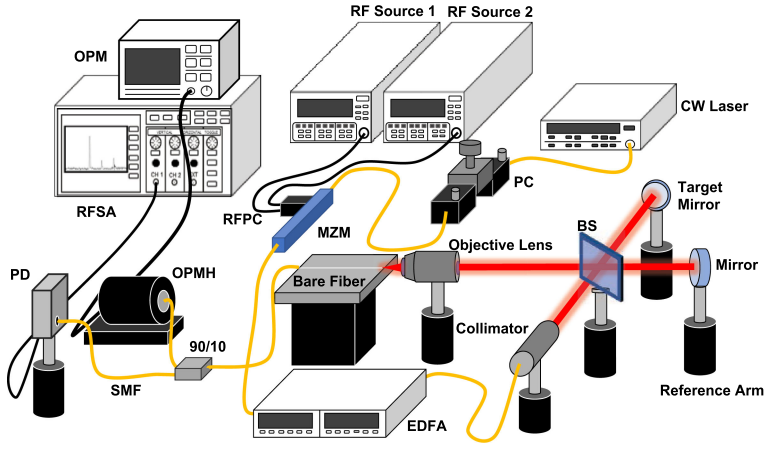

Fig. 4. Full experimental setup.

last portion of true range information (L_{act}) that can be represented as $L_{act} = N \times L_{rep} + L_f$, where L_{rep} is the distance of modulation pattern repetition and L_f is the final range information that can be extracted from this system. However, it is not possible to extract the number of repetitions (N) directly. Using quasi-CW signals can eliminate uncertainty and act as coarse range measurement. For instance, in the case of autonomous vehicles, the 300 m operation range requires 2 μs light propagation. The pulsed modulation with 100 kHz repetition rate and 50% duty cycle can yield sufficient time ($>$3 μs) to acquire enough data for averaging. Also, it is possible to further increase the data acquisition time by increasing the duty cycle or decreasing the repetition rate.

Figure 3 demonstrates how the modulation depth of the sinusoidal fit is decreasing while the backscattered signal is being attenuated with respect to the reference signal. There is a trade-off between the modulation depth and sensitivity of the system. When a high reference power is used, the coherent detection allows you to detect lower scattering powers, however, the variation between the constructive and destructive interference is mitigated. Therefore, the reference power should be optimized for the desired application based on the loss in the measurement arm that is due to divergence, range, and scattering efficiency.

3. Experimental Verification

To demonstrate the system performance, the proposed Lidar system is established on the optical table as shown in Fig. 4. We used a CW laser operating at 1550 nm with 14 mW average power.

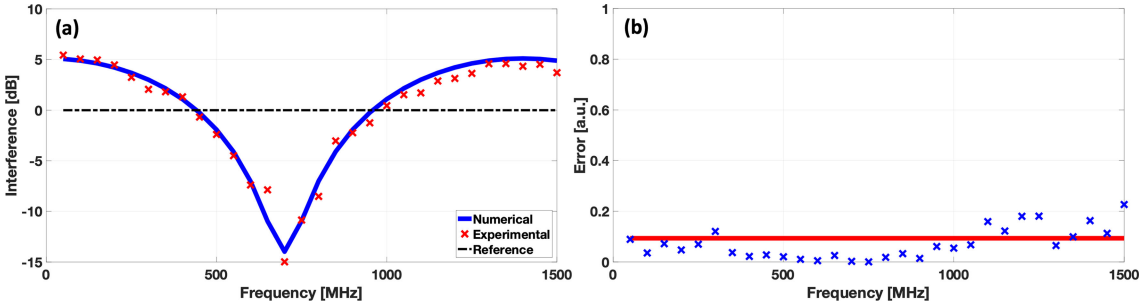

Fig. 5. (a) Frequency sweeping for a stationary target sitting at a fixed distance (10.71 cm). Intensities are normalized with respect to the reference signal. (b) The calculated error between experimental data and theoretical expectation for frequency sweeping.

The laser output is sent to an 8 GHz $LiNbO_3$ MZM to modulate light with the sum of two RF tones. Two RF tones generated by Agilent RF Signal Generators are combined with a coaxial 2-way power combiner (RFPC) and fed into modulator's RF port. Quadrature bias operation of the MZM is ensured by a DC power supply. The modulated light is first amplified by an Erbium doped fiber amplifier (EDFA) with 10 dB gain and transferred to the free space via a collimator with 2.1 mm beam waist and 0.95 mrad beam divergence. The transmitted beam is further split into two through a non-polarizing 50-50 beam splitter (BS) cube. In this experiment, for demonstration purposes, we used Aluminum mirrors with $>$95% reflectivity as a target and reference, hence $\alpha_{ref} \approx \alpha_m \approx 1$. The target mirror is translated on an optical rail for coarse measurements, then on an integrated micrometer stage for fine tuning. The current setup is used for the proof of principle of ranging only, therefore the target is stationary and not yielding any Doppler shifts for speed profiling. However, the velocimetry capability of a similar configuration is recently demonstrated for an oscillating target [41]. The back-reflected signals from the mirrors are recombined on the same beam splitter and directed to the heterodyne detection mechanism. As a detector, we used a fiber coupled InGaAs PIN photodiode (PD) with $>$12.5 GHz bandwidth. For these proof of concept experiments, it is sufficient to use a PIN photodiode, which has an active area diameter of 32 μm that can detect as low as $>$5 μW. Since such a high bandwidth requires small active area, which reduces the sensitivity of the detector, in a more realistic system an avalanche photodetector (APD) should be considered to enhance the detection capability by three orders of magnitude. A free space to fiber coupling system is built with a coupling efficiency $>$25%, by utilizing 3D micrometer stages and a 10$\times$ objective lens with a numerical aperture of 0.25. After coupling to the fiber, through a 90/10 power splitter, the average power is observed through an optical power meter (OPM), while spectral measurements are performed by an RF Spectrum Analyzer (RFSA). The acquired spectra are recorded and further post-processed in MATLAB to extract the range information via sinusoidal fitting algorithms.

4. Results and Discussion

For proof of concept demonstration, two experiments are performed: (i) frequency sweeping of a stationary target anchored at a fixed distance and (ii) measuring the powers of two tones for a target that is placed at different distances.

Figure 5(a) demonstrates the frequency sweeping of a target at fixed range, where red dots represent the experimental data points and blue curve the numerical expectation. The two consecutive peaks are observed at DC and 1.4 GHz indicating $\Delta f = 1.4\,\text{GHz} \rightarrow \frac{c}{2\Delta f} = 10.71\,\text{cm}$, along with the destructive interference occurring at the 700 MHz tone. Due to a greater loss in the measurement arm, where $\alpha_m/\alpha_{ref} = 0.8$, constructive interference is achieved as $\sim$5.1 dB higher than the reference. As is clear, the experimental data are well matched with the numerical analysis. The

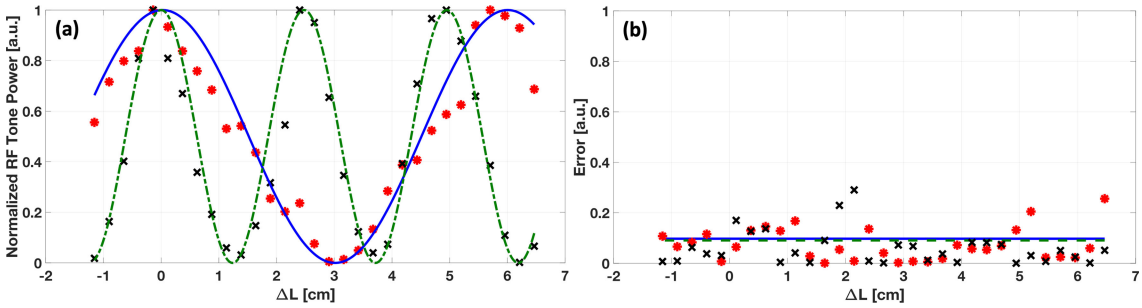

Fig. 6. (a) Multi-tone measurement by using two tones at 2.5 GHz and 6 GHz (b) Calculated error between experimental data and theoretical expectation for individual tones at 2.5 GHz (dots) and 6 GHz (crosses) in the multi-tone measurement system. RMS error values at 2.5 GHz and 6 GHz are represented as solid and dashed lines respectively.

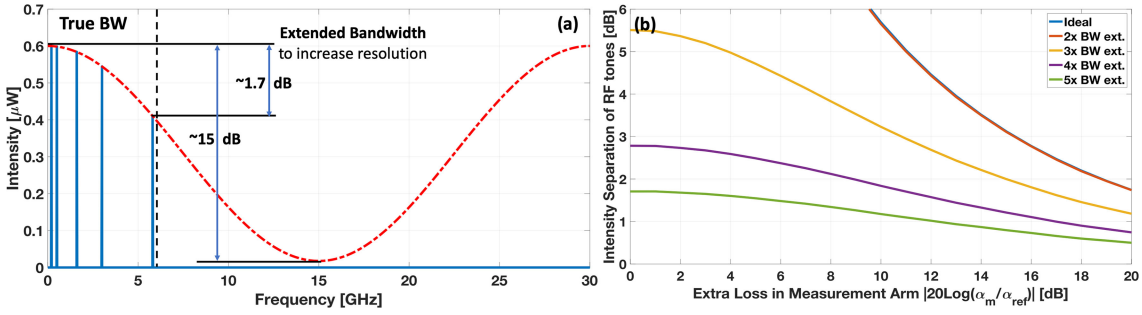

Fig. 7. (a) Five times extended bandwidth to increase the resolution through sine fitting algorithm (b) Suppression of the variation between RF tone intensities during bandwidth extension up to five times.

mismatch between the experiment and the numerical expectation is shown in Fig. 5(b), where the root-mean-square (RMS) error is calculated as 0.0936.

This experiment is used as a calibration for the proposed MTCW Lidar system. Since, several components in the experimental setup, such as RF path and MZM, have frequency dependency, the detected signal amplitudes have variations across the RF frequencies due to these imperfections. To eliminate such variations, we normalized the acquired interference powers with respect to the reference signal power that is measured while blocking the measurement arm. In Fig. 5(a), 0 dB line shows the reference signal power. In the complete system, after system calibration, pre-distortion can be applied to the tones to equate the power levels and eliminate the need for calibration experiment.

In the second experiment, we modulate the CW laser by using two RF tones at 2.5 GHz and 6 GHz, and the measurement arm is moved slowly to observe the interference. Fig. 6(a) shows that 2.5 GHz and 6 GHz tones are forming waveforms with 6 cm and 2.5 cm periods, respectively. The results are in a perfect correlation with the theoretical expectations. Fig. 6(b) indicates the amount of error in the system at each measurement distance for individual tones. The RMS error of the system is calculated from the error graph as 0.0972 and 0.0905 for 2.5 GHz and 6 GHz tones, respectively.

We note that 6 GHz RF bandwidth is sufficient to resolve 2.5 cm with a full cycle. It is also possible to add more tones at lower frequencies without increasing the total RF bandwidth of 6 GHz and further applying signal processing to achieve higher resolution. Fig. 7(a) demonstrates 5 mm range resolution by applying curve fitting and data extrapolation. Normally, 30 GHz RF bandwidth is required to achieve 5 mm resolution. However, extending the bandwidth or improving the resolution through data extrapolation is possible if the SNR of the detected signal is high enough. The behavior of the system for different ranges of extrapolation for a higher resolution can be seen in Fig. 7(b).

As we extrapolate the fit based on a few low-frequency tones, the amplitude difference between these tones becomes very crucial. The ideal case (full cycle) and the 2× bandwidth extension (half cycle) results are overlapping as shown in Fig. 7(b). This is due to true bandwidth's capability of capturing constructive interference at low frequencies and destructive at high. For bandwidth efficiency purposes, careful selection of RF tones plays a significant role. Then, it is possible to utilize the double bandwidth entirely without facing any penalties. Further improvements can be performed depending on the SNR and modulation depth of the detected signal. The SNR depends on the incident beam power, detector sensitivity and divergence of the beam. In the actual practice, utilizing a high average output power laser and increasing the collection efficiency via carefully engineered collection optics will enhance the signal strength along with an amplified APD. In addition, it is also possible to increase the signal level by applying RF heterodyning after the optical detector.

5. Conclusion

In this work, we demonstrate the multi-tone modulated continuous wave Lidar system. The technique has the capability of providing high precision range and velocity information of static and moving targets. In addition, we performed proof of concept experiments along with the theoretical and numerical analysis of range measurements in a static environment. Further applications of the proposed method for scattering or moving targets can be implemented by engineering the source power, receiver sensitivity and utilizing the Doppler frequency shift.

Acknowledgment

The authors wish to thank the anonymous reviewers for their valuable suggestions.

References

[1] B. L. Stann, W. C. Ruff, and Z. G. Sztankay, "Intensity-modulated diode laser radar using frequency-modulation/continuous-wave ranging techniques," *Opt. Eng.*, vol. 35, no. 11, pp. 3270–3279, Nov. 1996.
[2] A. Ansmann, U. Wandinger, M. Riebesell, C. Weitkamp, and W. Michaelis, "Independent measurement of extinction and backscatter profiles in cirrus clouds by using a combined Raman elastic-backscatter lidar," *Appl. Opt.*, vol. 31, no. 33, pp. 7113–7131, Nov. 1992.
[3] A. Braun, C. Y. Chien, S. Coe, and G. Mourou, "Long range, high resolution laser radar," *Opt. Commun.*, vol. 105, no. 1, pp. 63–66, Jan. 1994.
[4] J. L. Bufton, J. B. Garvin, J. F. Cavanaugh, L. A. Ramos-Izquierdo, T. D. Clem, and W. B. Krabill, "Airborne lidar for profiling of surface topography," *Opt. Eng.*, vol. 30, no. 1, pp. 72–79, Jan. 1991.
[5] A. Ansmann and D. Müller, "Lidar and atmospheric aerosol particles," in *Lidar: Range-Resolved Optical Remote Sensing of the Atmosphere*, C. Weitkamp, Ed. New York, NY, USA: Springer-Verlag, 2005, pp. 105–141.
[6] R.-E. Mamouri and A. Ansmann, "Potential of polarization/Raman lidar to separate fine dust, coarse dust, maritime, and anthropogenic aerosol profiles," *Atmospheric Meas. Tech.*, vol. 10, no. 9, pp. 3403–3427, Sep. 2017.
[7] P. P. Sullivan, C.-H. Moeng, B. Stevens, D. H. Lenschow, and S. D. Mayor, "Structure of the entrainment zone capping the convective atmospheric boundary layer," *J. Atmospheric Sci.*, vol. 55, no. 19, pp. 3042–3064, Oct. 1998.
[8] J. Quan *et al.*, "Evolution of planetary boundary layer under different weather conditions, and its impact on aerosol concentrations," *Particuology*, vol. 11, no. 1, pp. 34–40, Feb. 2013.
[9] T. Luettel, M. Himmelsbach, and H. Wuensche, "Autonomous ground vehicles—concepts and a path to the future," *Proc. IEEE*, vol. 100, no. Special Centennial Issue, pp. 1831–1839, May 2012.
[10] M. Himmelsbach, A. Müller, T. Luettel, and H. J. Wuensche, "LIDAR-based 3D object perception," in *Proc. 1st Int. Workshop Cognit. Tech. Syst.*, 2008.
[11] S. Ramasamy, R. Sabatini, A. Gardi, and J. Liu, "LIDAR obstacle warning and avoidance system for unmanned aerial vehicle sense-and-avoid," *Aerosp. Sci. Technol.*, vol. 55, pp. 344–358, Aug. 2016.
[12] K. Kidono, T. Miyasaka, A. Watanabe, T. Naito, and J. Miura, "Pedestrian recognition using high-definition LIDAR," in *Proc IEEE Intell. Veh. Symp.*, 2011, pp. 405–410.
[13] R. Aufrere, J. Gowdy, C. Mertz, C. Thorpe, C. C. Wang, and T. Yata, "Perception for collision avoidance and autonomous driving," *Mechatronics*, vol. 13, no. 10, pp. 1149–1161, Dec. 2003.
[14] P. Y. Shinzato, D. F. Wolf, and C. Stiller, "Road terrain detection: Avoiding common obstacle detection assumptions using sensor fusion," in *Proc. 2014 IEEE Intell. Vehicles Symp. Proc.*, 2014, pp. 687–692.
[15] Z. Chen *et al.*, "Accuracy improvement of imaging lidar based on time-correlated single-photon counting using three laser beams," *Opt. Commun.*, vol. 429, pp. 175–179, Dec. 2018.

[16] J. P. Godbaz, M. J. Cree, A. A. Dorrington, and A. D. Payne, "A fast maximum likelihood method for improving AMCW lidar precision using waveform shape," in *Proc IEEE SENSORS*, 2009, pp. 735–738.
[17] J. P. Godbaz, M. J. Cree, and A. A. Dorrington, "Understanding and ameliorating non-linear phase and amplitude responses in AMCW lidar," *Remote Sens.*, vol. 4, no. 1, pp. 21–42, Dec. 2011.
[18] D. J. Lum, S. H. Knarr, and J. C. Howell, "Frequency-modulated continuous-wave LiDAR compressive depth-mapping," *Opt. Exp.*, vol. 26, no. 12, Jun. 2018, Art. no. 15420.
[19] B. Behroozpour, P. A. M. Sandborn, M. C. Wu, and B. E. Boser, "Lidar system architectures and circuits," *IEEE Commun. Mag.*, vol. 55, no. 10, pp. 135–142, Oct. 2017.
[20] M.-C. Amann, T. M. Bosch, M. Lescure, R. A. Myllylae, and M. Rioux, "Laser ranging: A critical review of unusual techniques for distance measurement," *Opt. Eng.*, vol. 40, no. 1, pp. 10–20, Jan. 2001.
[21] P. McManamon, *Field Guide to Lidar*. Bellingham, WA, USA: SPIE, 2015.
[22] R. Whyte, L. Streeter, M. J. Cree, and A. A. Dorrington, "Application of lidar techniques to time-of-flight range imaging," *Appl. Opt.*, vol. 54, no. 33, pp. 9654–9664, Nov. 2015.
[23] A. D. Payne, A. A. Dorrington, M. J. Cree, and D. A. Carnegie, "Improved measurement linearity and precision for AMCW time-of-flight range imaging cameras," *Appl. Opt.*, vol. 49, no. 23, pp. 4392–4403, Aug. 2010.
[24] A. A. Dorrington, M. J. Cree, A. D. Payne, R. M. Conroy, and D. A. Carnegie, "Achieving sub-millimetre precision with a solid-state full-field heterodyning range imaging camera," *Meas. Sci. Technol.*, vol. 18, no. 92007, Art. no. 2809.
[25] E. Yoshikawa and T. Ushio, "Wind ranging and velocimetry with low peak power and long-duration modulated laser," *Opt. Exp.*, vol. 25, no. 8, pp. 8845–8859, Apr. 2017.
[26] P. Feneyrou *et al.*, "Frequency-modulated multifunction lidar for anemometry, range finding, and velocimetry—2. Experimental results," *Appl. Opt.*, vol. 56, no. 35, pp. 9676–9685, Dec. 2017.
[27] T. Hariyama, P. A. M. Sandborn, M. Watanabe, and M. C. Wu, "High-accuracy range-sensing system based on FMCW using low-cost VCSEL," *Opt. Exp.*, vol. 26, no. 7, pp. 9285–9297, Apr. 2018.
[28] P. Sandborn, N. Kaneda, Y.-K. Chen, and M. C. Wu, "Dual-sideband linear FMCW lidar with homodyne detection for application in 3D imaging," in *Proc Con. Lasers Electro-Opt.*, 2016, Paper STu4H.8.
[29] P. A. M. Sandborn, T. Hariyama, and M.-C. Wu, "Resolution-enhancement for wide-range non-linear FMCW lidar using quasi-synchronous resampling," in *Proc. Imag. Appl. Opt.*, 2017, Paper DW3F.3.
[30] T. Kim, P. Bhargava, and V. Stojanovic, "Optimal spectral estimation and system trade-off in long-distance frequency-modulated continuous-wave lidar," in *Proc. IEEE Int. Conf. Acoust., Speech Signal Process.*, 2018, pp. 1583–1587.
[31] T. W. D. Bosq and B. L. Preece, "Frequency modulated continuous wave lidar performance model for target detection," *Proc. SPIE*, vol. 10178, 2017, Art. no. 101780T.
[32] O. Batet, F. Dios, A. Comeron, and R. Agishev, "Intensity-modulated linear-frequency-modulated continuous-wave lidar for distributed media: fundamentals of technique," *Appl. Opt.*, vol. 49, no. 17, pp. 3369–3379, Jun. 2010.
[33] P. Trocha *et al.*, "Ultrafast optical ranging using microresonator soliton frequency combs," *Science*, vol. 359, no. 6378, pp. 887–891, Feb. 2018.
[34] M. Gupta, A. Velten, S. K. Nayar, and E. Breitbach, "What are optimal coding functions for time-of-flight imaging?," *ACM Trans. Graph. TOG*, vol. 37, no. 2, 2018, Art. no. 13.
[35] F. Li, J. Yablon, A. Velten, M. Gupta, and O. Cossairt, "High-depth-resolution range imaging with multiple-wavelength superheterodyne interferometry using 1550-nm lasers," *Appl. Opt.*, vol. 56, no. 31, pp. H51–H56, 2017.
[36] R. Dändliker, R. Thalmann, and D. Prongué, "Two-wavelength laser interferometry using superheterodyne detection," *Opt. Lett.*, vol. 13, no. 5, pp. 339–341, 1988.
[37] C. S. Bamji *et al.*, "A 0.13 μm CMOS system-on-chip for a 512 $\times$ 424 time-of-flight image sensor with multi-frequency photo-demodulation up to 130 MHz and 2 GS/s ADC," *IEEE J. Solid-State Circ.*, vol. 50, no. 1, pp. 303–319, Jan. 2014.
[38] R. D. Peters, O. P. Lay, S. Dubovitsky, J. Burger, and M. Jeganathan, "Design considerations and validation of the MSTAR absolute metrology system," *Proc. SPIE*, vol. 5531, pp. 32–44, 2004.
[39] L. Mandel, "Complex representation of optical fields in coherence theory," *J. Opt. Soc. Amer.*, vol. 57, no. 5, pp. 613–617, May 1967.
[40] E. I. Ackerman and C. H. Cox, "Effect of pilot tone-based modulator bias control on external modulation link performance," in *Proc. Int. Top. Meeting Microw. Photon*, 2000, pp. 121–124.
[41] M. M. Bayer, R. Torun, I. U. Zaman, and O. Boyraz, "A basic approach for speed profiling of alternating targets with photonic doppler velocimetry," in *Proc. Conf. Lasers Electro-Opt.*, 2019, Paper AW4K.4.